Available online at www.sciencedirect.com
ScienceDirect
Journal of Sound and Vibration 315 (2008) 258–278
JOURNAL OF SOUND AND VIBRATION
www.elsevier.com/locate/jsvi

Response of turbine flow meters to acoustic perturbations

P.W. Stoltenkamp[a,*], J.T.M. Bergervoet[b], J.F.H. Willems[a], F.M.R. van Uittert[a], A. Hirschberg[a]

[a]*Fluid Dynamics Laboratory, Department of Applied Physics, Eindhoven University of Technology, Building Cascade, P.O. Box 513, 5600 MB Eindhoven, The Netherlands*
[b]*Elster Instromet B.V., P.O. Box 7, 7064 ZG Silvolde, The Netherlands*

Received 25 April 2007; received in revised form 15 January 2008; accepted 17 January 2008
Handling Editor: P. Joseph
Available online 14 March 2008

Abstract

Acoustic pulsations can have a significant effect on gas turbine flow meters during volume flow measurements. These systematic errors are investigated experimentally for high-frequency pulsations and are compared to the results of a quasi-steady theory. Although significant deviations were found from the quasi-steady theory, the quadratic dependence of the velocity amplitude appears to remain valid for all measurements. The exact quadratic dependence is a function of Strouhal number of the pulsations. In the range of Strouhal numbers below 2.5, based on the chord length at the tip of the rotor blade and the flow velocity at the rotor inlet plane, we find a slow decrease in the error with increasing Strouhal number, *Sr*. The shape of the leading edge of the rotor blades does not affect this behaviour.

1. Introduction

Gas turbine flow meters can reach high accuracy, generally of the order of 0.2%. This accuracy can only be attained for optimal flow conditions. Acoustic perturbations resulting into flow pulsations can induce significant systematic errors. A theoretical prediction of the error would allow a correction in the volume flow measurement. The errors we consider in this paper are due to nonlinearities.

In recent years research has been carried out to determine the pulsation error during the measurement and correct for this error. Atkinson [1] developed a software tool to solve the equation of motion of the rotor and used the magnetic pickup registering the passing of a rotor blade to calculate the actual volume flow. This method can only be used if the pulsations can still be detected in the turbine signal. As the pulsations in the turbine meter signal decreases rapidly with increasing frequency, it is difficult to predict the real flow for high-frequency pulsations. Another tool was developed by Cheesewright et al. [2], called the 'Watchdog System'. This system also uses the equation of motion of the rotor. Watchdog is designed for pulsation frequencies less than 2 Hz. We actually focus on the behaviour of the rotor at high frequencies for which the rotor inertia has integrated fluctuations out. The rotor speed is therefore constant.

*Corresponding author.
E-mail address: stoltenkamp@hotmail.com (P.W. Stoltenkamp).

0022-460X/$ - see front matter © 2008 Elsevier Ltd. All rights reserved.
doi:10.1016/j.jsv.2008.01.051

Assuming quasi-steady, incompressible flow and neglecting friction forces a relationship can be found between the velocity pulsations and the measurement error [3]. Experiments have been carried out in the past by Lee et al. [4], Jungowski and Weiss [5], Cheesewright et al. [2] and McKee [6]. These experiments indicated that this basic theory can be used for low-frequency pulsations. To explore the limits of the validity of this theory, a set-up was built at the Eindhoven University of Technology. In particular we address the question whether pulsation errors still exist at high Strouhal numbers and how errors due to acoustical perturbations of different frequencies interact.

In our experiments care was taken to determine accurately the amplitude of the velocity fluctuations at the rotor. This was found to be a limitation in the earlier experiments reported in as literature. With the more accurate determination of the acoustic field it is possible to detect small deviations from the basic theory. With this set-up it was possible to measure the influence on the response of a flow meter (4″ diameter) of the acoustic perturbation with velocity amplitudes from 2% to 200% of the main flow velocity for frequencies from 24 up to 730 Hz. The range of Strouhal numbers was based on the blade length: $2 \times 10^{-2} \leqslant Sr_{L_{\text{blade}}} \leqslant 10$ (see Eq. (24).

2. Theoretical modelling

2.1. A two-dimensional quasi-steady model for a rotor with infinitesimally thin blades in incompressible flow

If the rotor is modelled as a two-dimensional cascade of infinitesimally thin blades in an incompressible, frictionless, steady flow, the integral mass and momentum equation applied to a fixed control surface CS with an outer normal $\mathbf{n}$ reduces to

$$\rho_0 \iint_{\text{CS}} \mathbf{v} \cdot \mathbf{n} \, \mathrm{d}S = 0, \tag{1}$$

$$\rho_0 \iint_{\text{CS}} \mathbf{v}(\mathbf{v} \cdot \mathbf{n}) \, \mathrm{d}S = \mathbf{F}_{\text{bf}}, \tag{2}$$

where ρ_0 is the fluid density, $\mathbf{v}$ is the velocity vector and $\mathbf{F}_{\text{bf}}$ are the forces imposed on the fluid by the turbine blades. The control volume, CS, is chosen as shown in Fig. 1. Because infinitesimally thin blades and frictionless flow are assumed, the surface area of inflow is equal to the surface area of outflow. It follows from Eq. (1) that the axial component of the incoming velocity, u_{in}, is equal to the outgoing velocity, $u_{\text{out},x}$; $u_{\text{in}} = u_{\text{out},x}$.

It is assumed that the flow enters the rotor without any angular momentum and that the flow leaves the rotor with a velocity aligned with the blades (see Fig. 1). This is a realistic assumption if the chord length of the blades, L_{blade}, is large compared to the distances between the blades, s, i.e. for cascades, the ratio, s/L_{blade}, should be less than 0.7 [7].

By considering the flow in a reference frame attached to the rotor, this implies that

$$\tan\beta = \frac{\omega r + u_{\text{out},y}}{u_{\text{out},x}}. \tag{3}$$

We assume further that there is no swirl in the incoming flow so that $u_{\text{in},y} = 0$ and that the inflow is uniform. The momentum equation in the y-direction can be approximated by

$$\rho_0 A u_{\text{in}}(u_{\text{in}} \tan\beta_{\text{av}} - \omega R) = F_{\text{bf},y}, \tag{4}$$

where ω is the angular rotation velocity of the rotor, A is the cross-sectional area of the rotor, β_{av} is the average blade angle and R is the root-mean-square radius of the inner and outer radii of the meter, r_{in} and r_{out}, i.e., $R = \sqrt{\frac{1}{2}(r_{\text{in}}^2 + r_{\text{out}}^2)}$. The force exerted on the fluid by the blade, $F_{\text{bf},y}$, is equal and opposite to the force exerted by the fluid on the blade, $F_{\text{fb},y}$. The fluid induces a torque on the rotor, $T_{\text{fb}} = F_{\text{fb},y}R$, accelerating the rotor. Using the equation of motion of the rotor, we get

$$I_{\text{rotor}} \frac{\mathrm{d}\omega}{\mathrm{d}t} = \rho_0 A u_{\text{in}}(u_{\text{in}} \tan\beta_{\text{av}} - \omega R)R - T_f, \tag{5}$$

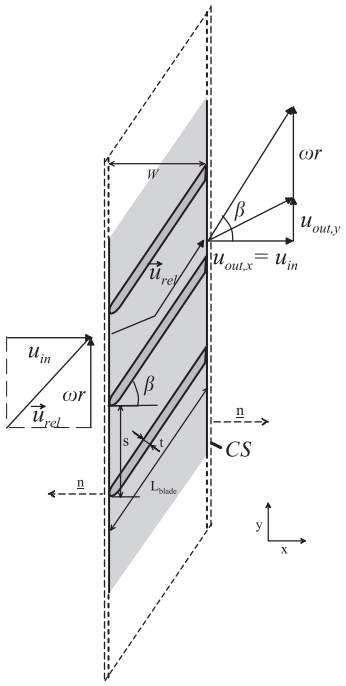

Fig. 1. Two-dimensional representation of the flow entering and leaving the rotor modelled as a cascade.

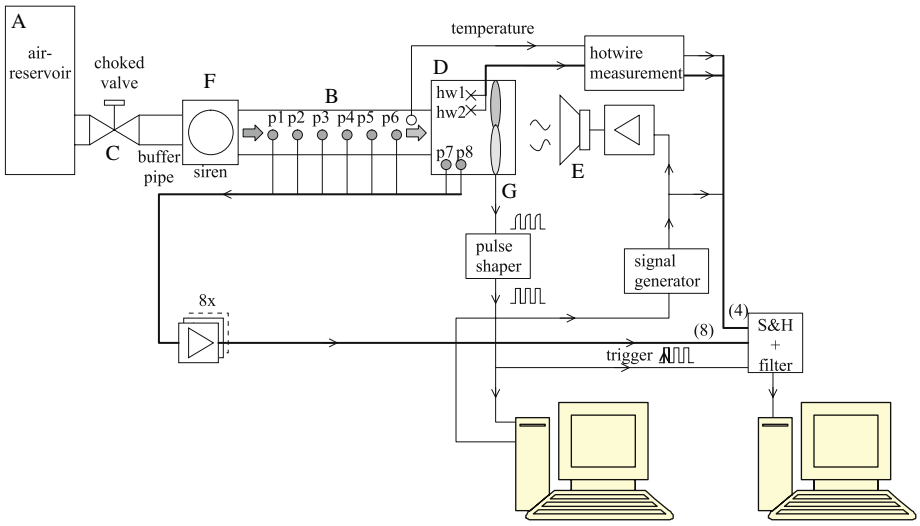

Fig. 2. Experimental set up: a high-pressure reservoir of dry air (A) is connected with a pipe (B) to a turbine meter (D). The flow is controlled by an adjustable valve (C) creating choked flow with constant mass flow. Pulsations can be induced by a loudspeaker (E) or a siren (F). The pulsations are measured with six pressure transducers ($p1, p2, p3, p4, p5$ and $p6$) along in the test pipe (B) and two pressure transducers ($p7$ and $p8$) placed within the turbine meter (D). Velocity pulsations can be measured with two hot wires (hw1 and hw2) placed within the turbine meter (D). The rotation of the rotor of the turbine meter is measured by a probe detecting the passing of a rotor blade (G).

where I_{rotor} is the moment of inertia of the rotor and T_f is torque on the rotor caused by the friction forces (Fig. 2).

We assume periodic pulsations u'_{in} around an average velocity $\bar{u}_{\text{in}}$ so that $u_{\text{in}} = \bar{u}_{\text{in}} + u'_{\text{in}}$. We neglect the friction torque, because $T_{\text{f}}/(\rho u_{\text{in}}^2 R^3) \ll 1$. We assume that the rotation of the rotor is constant in spite of the pulsations. This implies that the response time of the rotor is much longer than the period, T, of the imposed

acoustic pulsations, $(I_{\text{rotor}}/T\rho_0 u_{\text{in}}^2 A) \gg 1$. If the torque is averaged over one pulsation period, Eq. (5) reduces to

$$\frac{1}{T}\int_0^T \rho_0(\bar{u}_{\text{in}}+u'_{\text{in}})A[(\bar{u}_{\text{in}}+u'_{\text{in}})\tan\beta_{\text{av}}-\omega R]R\,\mathrm{d}t = \rho_0 AR[(\bar{u}_{\text{in}}^2+\overline{u'^2_{\text{in}}})\tan\beta_{\text{av}}-\overline{\bar{u}_{\text{in}}\omega R}] = 0, \tag{6}$$

because $\overline{u'_{\text{in}}} = 0$. The density fluctuations ρ'/ρ_0 are of the order of u'_{in}/c_0, where c_0 is the speed of sound. As $\overline{u}_{\text{in}}/c_0 \ll 1$ we have that $\rho'/\rho_0 \ll u'_{\text{in}}/\overline{u}_{\text{in}}$ and we can neglect density fluctuations. Please note furthermore that $u'_{\text{in}}/\overline{u}_{\text{in}}$ is not necessarily small. The effect of pulsations with high amplitudes is discussed by Cheesewright et al. [8]. From this equation the angular rotation velocity, $\bar{\omega}$, caused by pulsating flow is obtained:

$$\bar{\omega} = \frac{\bar{u}_{\text{in}}\tan\beta_{\text{av}}}{R}\left(1+\frac{\overline{u'^2_{\text{in}}}}{\bar{u}_{\text{in}}^2}\right). \tag{7}$$

Using $\omega_{\text{id}} = (\bar{u}_{\text{in}}\tan\beta_{\text{av}}/R)$ for the ideal angular rotation velocity without pulsation, the error caused by periodic pulsations becomes

$$(E_{\text{puls}})_{\text{id}} = \frac{\bar{\omega}-\omega_{\text{id}}}{\omega_{\text{id}}} = \left(\frac{\overline{u'^2_{\text{in}}}}{\bar{u}_{\text{in}}^2}\right). \tag{8}$$

This means that sinusoidal pulsations, $u_{\text{in}} = \bar{u}_{\text{in}} + |u'_{\text{in}}|\sin(2\pi t/T)$, induce a systematic error of

$$(E_{\text{puls}})_{\text{id}} = \frac{1}{2}\left(\frac{|u'_{\text{in}}|}{\bar{u}_{\text{in}}}\right)^2. \tag{9}$$

2.2. Practical definition of pulsation error

In the previous section we defined a deviation $(E_{\text{puls}})_{\text{id}}$ between angular velocity, $\bar{\omega}$, for steady rotation and the ideal angular rotation velocity, ω_{id}, in absence of pulsations:

$$(E_{\text{puls}})_{\text{id}} = \frac{\bar{\omega}-\omega_{\text{id}}}{\omega_{\text{id}}}, \tag{10}$$

where $\omega_{\text{id}} = \bar{u}_{\text{in}}\tan\beta_{\text{av}}/R$. In experiments we use the steady angular velocity ω_0 reached in absence of pulsations as reference instead of ω_{id}. Hence

$$E_{\text{puls}} = \frac{\bar{\omega}-\omega_0}{\omega_0}. \tag{11}$$

In order to illustrate the difference between this ideal pulsation error, $(E_{\text{puls}})_{\text{id}}$, and the definition of the pulsation error used in the experiments, E_{puls}, we consider the influence of a constant mechanical friction torque, $\bar{T}_{\text{mech}}$ on an ideal rotor. Using Eq. (6) we find in absence of pulsations

$$\omega_0 = \omega_{\text{id}} - \frac{\bar{T}_{\text{mech}}}{\rho_0 AR^2\bar{u}_{\text{in}}}, \tag{12}$$

while due to pulsations we would reach a steady rotation of angular velocity:

$$\bar{\omega} = \frac{\bar{u}_{\text{in}}\tan\beta}{R}\left(1+\frac{\overline{u'^2_{\text{in}}}}{\bar{u}_{\text{in}}^2}\right) - \frac{\bar{T}_{\text{mech}}}{\rho_0 AR^2\bar{u}_{\text{in}}}. \tag{13}$$

Hence, we would predict a pulsation error

$$(E_{\text{puls}})_{\text{exp}} = \left(\frac{\omega_{\text{id}}}{\omega_0}\right)\frac{\overline{u'^2_{\text{in}}}}{\bar{u}_{\text{in}}^2}, \tag{14}$$

corresponding to $(E_{\text{puls}})_{\text{id}} = \overline{u'^2_{\text{in}}}/\bar{u}_{\text{in}}^2$ multiplied by a factor $\omega_{\text{id}}/\omega_0$.

Other reasons for a deviation between the ideal pulsation error, $(E_{\text{puls}})_{\text{id}}$, and the measured pulsation error, E_{puls} defined by Eq. (11), is the unsteadiness of the flow at high Strouhal numbers. Our aim is to provide quantitative information about this Strouhal number dependence.

3. Experimental set-up

A dedicated set-up has been built at Eindhoven University of Technology to study the influence of pulsations on gas turbine meters. A high-pressure reservoir with dry air at 60 bar (dew point $-40\,^{\circ}C$) is connected to a test pipe of 0.10 m diameter, and a length of 3.2 m. At the open end of this pipe a turbine flow meter (Instromet type SM-RI-X G250) is placed. The flow through the turbine flow meter is controlled by means of a valve placed at the upstream end of the test pipe. By adjusting this valve, the critical pressure at the valve is reached, resulting in a velocity, u^*, at the valve equal to the local speed of sound, c^*. Locally, we have a Mach number of unity, $M = u^*/c^* = 1$ and the so-called ''choked'' flow. This provides a constant mass flow, independent of perturbations in the flow downstream of the valve. The conditions of the reservoir, p_0 and T_0, and the valve opening determine the mass flow.

Pulsations in the test pipe downstream of the choked valve can be induced by using a loudspeaker placed at the downstream open end of the set-up or by means of a siren placed downstream of the valve. The loudspeaker (SP-250P) is controlled using a signal generator (Yokogawa FG120) driving a power amplifier (AIM WPA 301A). The siren is described by Peters [9]. The siren has a frequency range from a 10 up to 1000 Hz. A bypass allows variations in the ratio, u_{ac}/u_0, of acoustic velocity, u_{ac}, and the main flow velocity, u_0. The siren is a much more efficient sound source than the loudspeaker, by tuning it to the resonance frequencies of the set-up, the ratio of acoustic to main flow velocities, u_{ac}/u_0, can reach values up to 2. Between the siren and the valve a volume is placed, a buffer pipe with length 1.22 m and internal diameter 0.21 m. Except for the core of the pipe with a diameter of 0.05 m, this pipe is filled with porous material (Achiobouw acoustic foam D80). To avoid chocking at the siren, the opening of the bypass of the siren was increased before each series of experiments, while the siren was turned off, up to the point at which changes in volume flow could no longer be observed. In this case the bypass opening has become larger than the opening of the upstream valve and does not control the flow. The upstream valve is chocked and imposes a fixed mass flow through the system. Only measurements using a significantly larger opening of the bypass than this critical point are performed. Good agreement between the measurements using the loudspeaker and using the loudspeaker confirm that there was no chocking at the siren.

The acoustic pressure in the set-up is measured by means of eight piezo-electric gauges placed flush at the pipe wall. Six pressure transducers (three Kistler type 7031 and three PCB type 116A) are placed in the test pipe upstream of the turbine meter each at randomly chosen distances (see Table 1). Two other pressure transducers (PCB type 116A) are placed within the turbine meter, 0.010 and 0.040 m upstream of the rotor of the turbine meter (see Fig. 3). The signals from the pressure transducers are amplified using charge amplifiers (Kistler type 5011). They are acquired by means of a PC using an 8 channel Sample and Hold module (National Instrument SCXI 1180) and a DAC card (PCI MIO-16E-I) controlled by LabView software. The pressure transducer and charge amplifier combinations are calibrated in a different set-up. In this calibration set-up the transducer is placed next to a reference microphone flush in a closed end wall of a 1.0 m long

Table 1
Position of the pressure transducer placed in the set-up

Pressure transducer in pipe	Distance (m)
1	−1.566
2	−1.212
3	−0.960
4	−0.400
5	−0.265
6	−0.205
Pressure transducer in turbine meter	Distance (m)
7	0.07775
8	0.1075

The distances are measured from the upstream end of the turbine meter, where the positive direction is the flow direction.

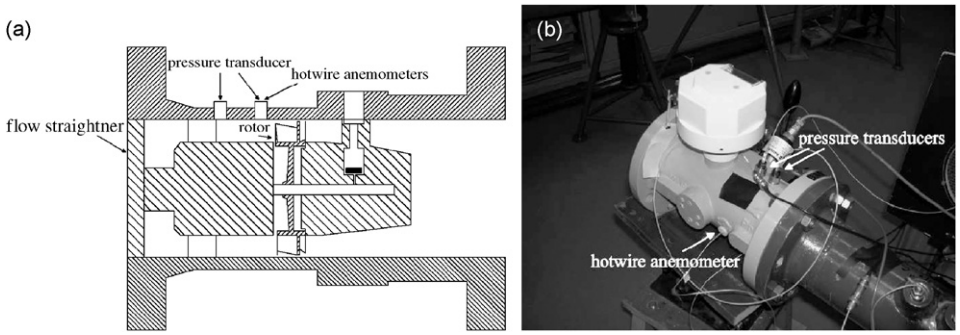

Fig. 3. The placement of the pressure transducers in the turbine meter: (a) shows a schematic, simplified drawing of a cross-section of the turbine flow meter and (b) shows a photograph of the turbine meter. One pressure transducer and two hot wires are placed at the same distance upstream from the rotor (1 cm), equally distributed around the perimeter of the meter.

pipe (diameter 0.07 m). Plane waves are generated by a loudspeaker placed at the opposite end of the pipe. All pressure transducers are calibrated against the reference pressure transducer for frequencies between 24 and 730 Hz, i.e. the frequencies used in our experiments. The acoustic velocity of the pulsations can also be measured using two hot wire anemometers (Dantec type 55P11 wire diameter 5 μm with 55H20 support) placed 0.010 m upstream of the turbine meter (see Fig. 3). Accurate measurements of the amplitude of the velocity pulsations by means of these hot wires are only possible if the ratio between the acoustic velocity amplitude and the main flow velocity is small enough to avoid flow reversal, $u_{ac}/u_0 < 1$. The hot wire makes no distinction between forward and reversed flow. The signals of the hot wire anemometers are processed with a constant-temperature anemometer module (Streamline 90n10) in combination with dedicated Dantec application software. The anemometer can follow velocity fluctuations up to 50 kHz. The signals are recorded on a PC in the same way as the signals of the pressure transducers. The hot wire anemometers are calibrated against a Betz water micromanometer (±1 Pa) in a separate free-jet set up in the velocity range $2-40\,\mathrm{m\,s^{-1}}$. The output is fitted using a power-law description. This results in accuracies of about 1% for velocities above $8\,\mathrm{m\,s^{-1}}$ and of about 5% for velocities from 2 to $8\,\mathrm{m\,s^{-1}}$.

The time-averaged volume flow can be measured using the turbine flow meter (Instromet type SM-RI-X G250), using the calibration data provided by Elster-Instromet for normal flow conditions. In the absence of pulsations the volume flow measured has an accuracy of 0.2% in the range 6×10^{-3}–$1 \times 10^{-1}\,\mathrm{m^3\,s^{-1}}$. The rotation of the rotor of the turbine meter is detected by means of a so-called ''reprox probe'', a magnetic pickup generating an inductive pulse when a rotor blade passes the probe. These pulses are converted to electronic pulses and then modified into proper TTL pulses by means of the signal generator. The time interval between the TTL pulses is registered using a counter board (PCI 6250 NI), inserted in a PC, with an accuracy of 50 ns. These intervals are converted to the rotation period of the rotor by multiplying by the number of rotor blades ($n = 16$). Due to small differences in blade geometry the measured rotor speed is not constant during a rotation. An average rotor speed is calculated for each rotation.

4. Determination of the amplitude of the velocity pulsations at the location of the rotor

When the loudspeaker or the siren is turned on, velocity pulsations are generated. The velocity in the set-up can be described by the average main flow, $\bar{u}_{in}$, and a periodic fluctuating part, u'_{in}. To investigate the effect of the acoustic perturbations on the flow measurements of the turbine meter, it is necessary to determine the velocity pulsations at the position of the rotor. It is impossible to measure the velocity pulsations exactly at the rotor. The measured data has to be extrapolated to the rotor position. By using the measured pressure fluctuations obtained by the microphones, the acoustic velocity at the rotor is determined by using an acoustic model.

4.1. Acoustic model

For the acoustic model the test pipe including the turbine meter is divided into three parts with different cross-sectional areas (see Fig. 4). The first part is the pipe leading to the turbine meter with a diameter $D = 0.10\,\mathrm{m}$. The pipe has a cross-sectional area of $8.4 \times 10^{-3}\,\mathrm{m}^2$. As can be seen in Fig. 3 the core of the turbine meter has a complicated shape around the rotor. In the acoustical model, the turbine meter will be described as two cylindrical parts changing abruptly in cross-sectional areas.

The first part of the turbine meter is the front part of the flow straightener and has a length of 0.037 m and a cross-sectional area of $7.3 \times 10^{-3}\,\mathrm{m}^2$. The second part is the main part of the turbine meter and has a smaller cross-sectional area of $3.8 \times 10^{-3}\,\mathrm{m}^2$. It is assumed that the acoustic field can be described within each segment as plane waves for frequencies up to the critical frequency of the pipe, $f_c = c_0/(2D) \approx 1.7\,\mathrm{kHz}$. Harmonic plane waves are escribed by the d'Alembert solution of the one-dimensional equation:

$$p'_j(x,t) = \hat{p}_j(x)\mathrm{e}^{i2\pi ft} = p_j^+ \mathrm{e}^{i(2\pi ft - k_j^+ x)} + p_j^- \mathrm{e}^{i(2\pi ft + k_j^- x)}, \quad j = 1,2,3, \tag{15}$$

with $\hat{p}_j$ the complex amplitude and $f = 1/T$ the radial frequency. In this case of an uniform main flow, k_j^+ and k_j^- are the complex wavenumbers of the waves travelling in positive and negative direction, respectively. The wavenumbers are defined by

$$k_j^+ = \frac{2\pi f/c_0}{1+M} + (1-i)\alpha_d, \quad k_j^- = \frac{2\pi f/c_0}{1-M} + (1-i)\alpha_d. \tag{16}$$

The imaginary part of the wavenumber is associated with the damping caused by viscous-thermal effects. In a quiescent flow in smooth cylindrical pipes, damping of plane waves by viscous-thermal damping can be described by a damping coefficient [10–12]

$$\alpha_d = \frac{1}{r_j c_0}\sqrt{\nu\pi f}\left(1 + \frac{\gamma - 1}{\sqrt{Pr}}\right), \tag{17}$$

where r_j is the radius of pipe segment j, ν is the kinematic viscosity, γ is the Poisson's ratio and Pr is the Prandtl number. For air at room temperature and atmospheric pressure the following values are used: $\nu = 1.5 \times 10^{-5}\,\mathrm{m^2\,s^{-1}}$, $\gamma = 1.4$ and $Pr = 0.72$. Although this damping coefficient is deduced for quiescent flow, it provides a good approximation of the effect of damping when the acoustical viscous boundary layer, $\delta = \sqrt{\nu/\pi f}$, is thinner than the viscous sublayer $10\delta^+$ with $\delta^+ = \nu\sqrt{\rho/\tau_w}$ ([13–15]). If we use the δ^+ for smooth cylindrical pipes, we find that this is valid for our experiments for $f \geqq 100\,\mathrm{Hz}$. At lower frequencies damping has only a minor effect on the wave propagation in the test pipe, and hence the approximation is also reasonable.

At the abrupt transitions in cross-section the integral formulation of the conservation of mass flow, m', and total enthalpy, B' are used for compressible potential flow [16];

$$m'_1 = m'_2,$$

$$B'_1 = B'_2,$$

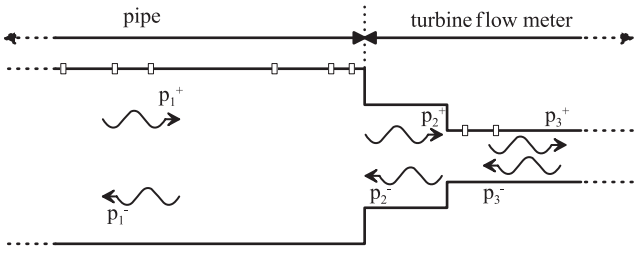

Fig. 4. A schematic illustration of the acoustic model used to determine the amplitude of the velocity pulsations at the position of the rotor.

$$m'_j = \frac{A_j}{c_0}(p_j^+ e^{-ik_j^+ x}(1+M_j) - p_j^- e^{ik_j^- x}(1-M_j)), \tag{18}$$

$$B'_j = \frac{1}{\rho_0}(p_j^+ e^{-ik_j^+ x}(1+M_j) + p_j^- e^{ik_j^- x}(1-M_j)). \tag{19}$$

By introducing a matrix $\mathbf{M}$ and a vector $[\mathbf{p_m}]$ with the pressures measured at the microphones, the solution of the system of the Eqs. (19) and (16) at the positions of the microphones can be computed. The system of equations becomes

$$\begin{bmatrix} p_j^+ \\ p_j^- \end{bmatrix} = (\mathbf{M}^T\mathbf{M})^{-1}\mathbf{M}^T \cdot [\mathbf{p_m}]. \tag{20}$$

From this system of equations the least-square solution of the plane wave amplitudes p_j^+ and p_j^- is determined. Using

$$u_{ac} = \frac{p_3^+ e^{-ik_3^+ x_r} - p_3^- e^{ik_3^- x_r}}{\rho_0 c_0}, \tag{21}$$

the velocity pulsations at the position of the rotor, x_r, is calculated.

4.2. Synchronous detection

To analyse the measured pressure signals synchronous detection, 'lock-in', is being used during post-processing. When the measurements are carried out by using a loudspeaker to induce pulsations, the signal driving the loudspeaker is used as reference. When the siren is used to induce pulsations, one of the pressure transducers is filtered out digitally using a second-order band-pass filter to produce a sinusoidal reference signal. From the sine wave reference signal a cosine wave signal is obtained by shifting the phase by $\pi/2$. The Hilbert transform routine of Matlab is used to obtain the shifted reference signal. The transducer signals are multiplied by the sine reference signal and integrated over a integer number of oscillation periods to extract the amplitude of the $\sin(2\pi ft)$ component of the signal. The same procedure is repeated for the cosine reference signal to obtain the amplitude of the $\cos(2\pi ft)$ component of the signal. Integration is done typically over a few hundred periods.

4.3. Verification of the acoustic model

To investigate the accuracy of the procedure for the determination of the acoustic velocity several approaches are used. The pressure transducers placed in the turbine meter are placed close to the rotor. The rotation of the rotor, the wake of the guiding vanes of the flow straightener and the abrupt transitions in cross-section can cause interference on these pressure measurements. This can be investigated by excluding the two microphones placed within the turbine meter. In Fig. 5 an example is given of an experiment in which pulsations were induced at 164 Hz. The figure shows the pressure amplitude, the added upstream and downstream travelling pressure waves. It can be found that the difference between these two models is small, in the order of a few percent in velocity amplitude, depending on frequency and standing wave pattern. This also indicates that acoustical dissipation due to the flow straightener just upstream of the flow meter can be neglected in our acoustical analysis.

The accuracy of the acoustic model depends on the position of the pressure nodes of the standing wave. If the pressure node is located around the rotor position, small deviations in the pressure wave induce small deviations in the velocity amplitude, because the acoustic velocity is rather uniform around a pressure node. When the rotor is close to a pressure antinode large errors in velocity amplitude can be induced by small deviations. Measurements are only considered when the acoustical velocity can be determined accurately. In Fig. 6 an example is given of a measurement at 362 Hz, for which the position of the rotor is close to a pressure anti-node. The results of this experiment were therefore not used in our analysis.

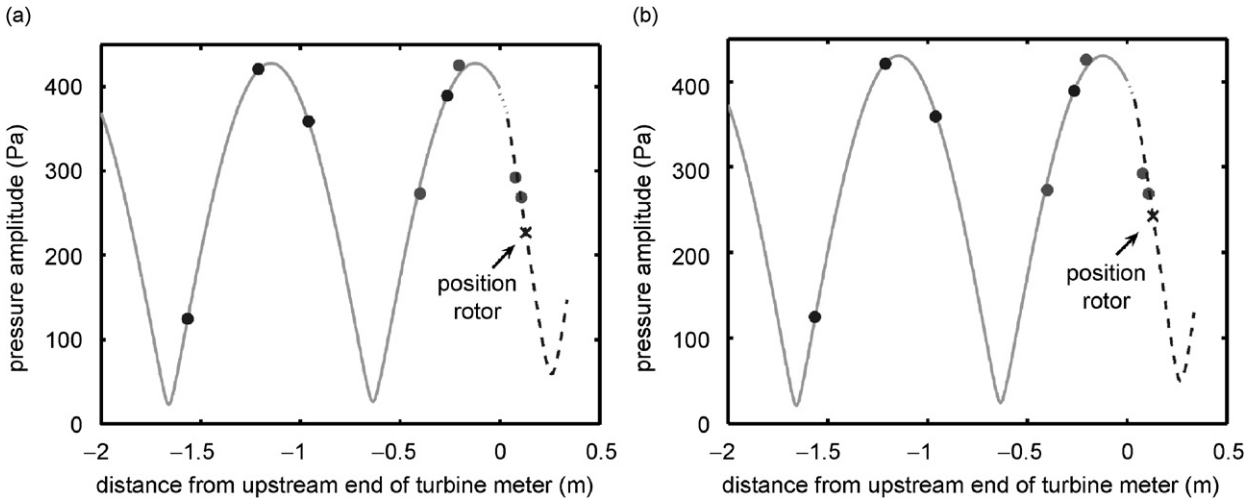

Fig. 5. The pressure amplitude of the standing wave in the set-up during a measurement at a frequency of $f = 164\,\text{Hz}$ with a mainstream velocity in the pipe of $u_0 = 2\,\text{m}\,\text{s}^{-1}$. The dots represent the measured pressure amplitude of the pressure transducers. (a) Shows a example of a measurement were all eight pressure transducers in the set up are used, (b) shows the standing wave predicted when the two pressure transducers in the turbine meter are not used. The different lines indicate the three different parts of the acoustic model (Fig. 4).

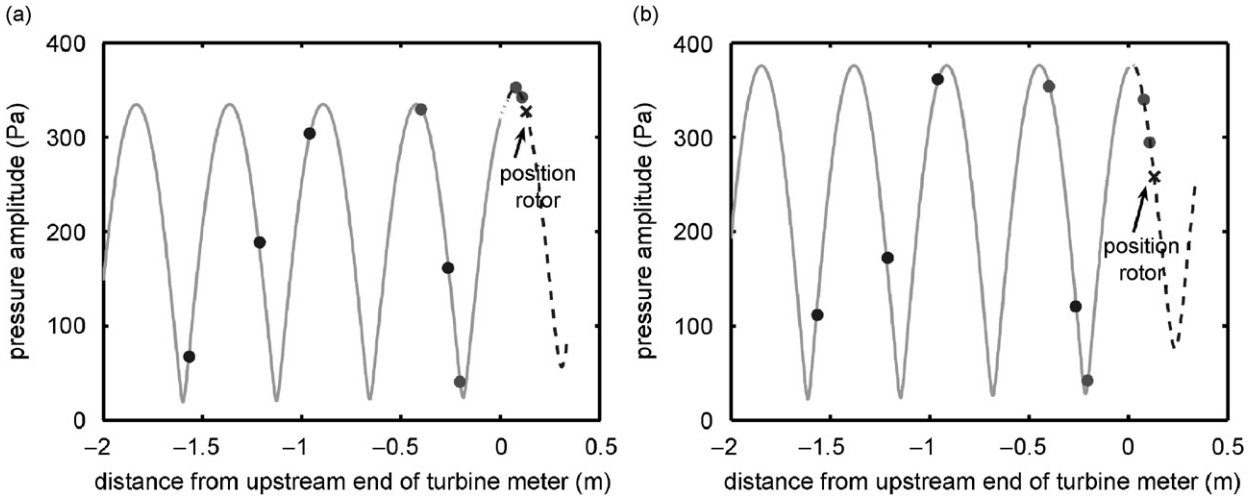

Fig. 6. The pressure amplitude of the standing wave in the set up for a measurement at a frequency of $f = 362\,\text{Hz}$ with a mainstream velocity in the pipe of $u_0 = 2\,\text{m}\,\text{s}^{-1}$. The dots represent the measured pressure amplitude of the pressure transducers. (a) Shows a example of a measurement where the rotor is located close to a pressure antinode, (b) shows a measurement at the same frequency and main stream velocity with the rotor not as close to the pressure maximum. The different lines indicate the three different parts of the acoustic model (Fig. 4).

To illustrate this, the velocity amplitude was calculated at the front of the rotor and at the back of the rotor (the rotor has a width of 2 cm). In the case shown in Fig. 6(a), where the rotor position is around a pressure antinode, the velocity amplitude changes over the width of the rotor by 28%, while in the Fig. 6(b) the velocity amplitude changes by 10%. Besides the location of the rotor position in respect to the standing wave, the frequency also plays an important roll. In Fig. 7 examples of a measurement at 24 Hz and a measurement at 730 Hz are shown. If we evaluate the accuracy as mentioned above, for 24 Hz the velocity amplitude changes over the rotor with less than 0.1%, while at 730 Hz this is about 3%. In this example (730 Hz) this change in velocity amplitude is still relatively small, because the rotor is positioned at a pressure node.

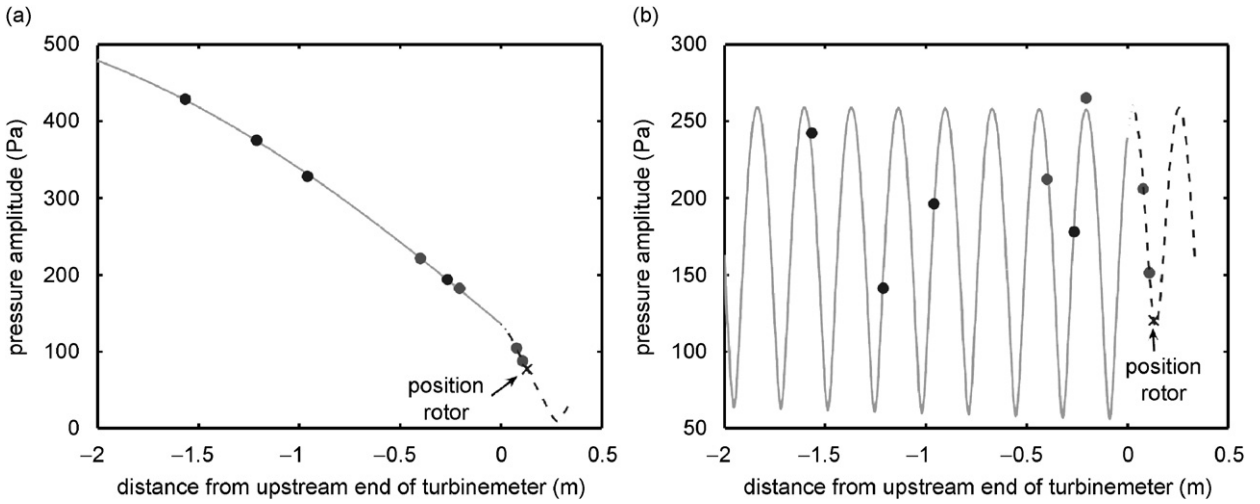

Fig. 7. The pressure amplitude of the standing wave in the set-up. The dots represent the measured pressure amplitude of the pressure transducers. (a) Shows a example of a measurement at 24 *rmHz*, (b) Shows a measurement at 730 Hz. Both measurements are carried out at a mainstream velocity $u_0 = 2\,\mathrm{m\,s^{-1}}$. The different lines indicate the three different parts of the acoustic model (Fig. 4).

To verify the velocity amplitude found with the acoustical model further, the velocity amplitude is measured 1 cm upstream of rotor by means of two hot wires placed at different positions. Two hot wires were used to account for the complicated flow profile behind the blades of the flow straightener. The local relative velocity pulsations for $|u'|/u_0 < 1$, can be compared with the relative velocity amplitude calculated with the acoustical model based on the pressure measurements. The measurements of the velocity amplitude with the hot wires are (within 10%) in agreement with the acoustical model for velocities higher than $2\,\mathrm{m\,s^{-1}}$. Below $2\,\mathrm{m\,s^{-1}}$ the calibration of the hot wire is problematic. We will discuss the hot wire measurements below.

The siren generates block pulses in volume flow, which drives many harmonics of the fundamental frequency. By using the siren at resonance frequencies of the pipe, the resonant frequency dominates over other frequencies. In that case we obtain an almost harmonic perturbation. Some overtones will, however, still be present. Using Eq. (9) it is expected that the contributions of the different harmonics add quadratically to the error:

$$E_{\mathrm{puls}} = \frac{1}{2}\left[\left(\frac{|u_1'|}{u_{\mathrm{in}}}\right)^2 + \left(\frac{|u_2'|}{u_{\mathrm{in}}}\right)^2 + \left(\frac{|u_3'|}{u_{\mathrm{in}}}\right)^2 + \cdots\right], \tag{22}$$

where the subscripts indicate the different harmonics. This is checked by inducing pulsations using the loudspeaker and the siren simultaneously at different frequencies. As is shown in Table 2 the measurement error, E_{add}, caused by the frequencies separately accumulates, to the measurement error caused by the two frequencies simultaneously, E_{sim}, within measurement accuracy. When the difference in frequency is small the induced acoustical velocity will display low-frequency beats which the siren can follow. This produces the type of signal shown in Fig. 8. As the frequency obtained by using the siren displays some drift in time, we observe some time dependence in the frequency of the beats for simultaneous measurements with two frequencies close together. As shown in Fig. 8 at $t = 20\,\mathrm{s}$ the loudspeaker is turned on and the turbine meter starts to measure a higher velocity. After another 20 s the siren is turned on, the measurement error becomes larger and starts oscillating. This is by the beats. Taking the time average of the error during the beats we still find that $E_{\mathrm{add}} \backsimeq E_{\mathrm{sim}}$ (Table 2).

For signals in which other frequencies are present, the contribution from each frequency can be added to predict the total error. As the error depends quadratically on the amplitude the harmonic with highest amplitude will dominate. In all the experimental results presented further the effect of frequencies other than the imposed fundamental frequency was less than 1% of the error signal E_{puls}.

Table 2
Measurements with pulsations at two frequencies

$\lvert u'\rvert/u_0$	$\lvert u'\rvert/u_0$	E_{add}	E_{sim}	$\frac{E_{sim}-E_{add}}{E_{sim}}\times 100\%$
$f=24\,\mathrm{Hz}$	$f=164\,\mathrm{Hz}$			
0.21	0.19	0.032	0.033	0.12%
0.21	0.33	0.074	0.074	−0.18%
0.21	0.57	0.227	0.228	0.64%
$f=164\,\mathrm{Hz}$	$f=367\,\mathrm{Hz}$			
0.09	0.07	0.005	0.005	−3.06%
0.09	0.12	0.011	0.010	−2.73%
0.09	0.16	0.015	0.016	1.04%
$f=164\,\mathrm{Hz}$	$f=166\,\mathrm{Hz}$			
0.26	0.18	0.036	0.040	6.17%
0.26	0.25	0.049	0.048	−1.07%
$f=164\,\mathrm{Hz}$	$f\approx 164\,\mathrm{Hz}$			
0.18	0.28	0.042	0.041	−2.32%
0.18	0.33	0.052	0.056	7.03%

E_{add} is the added measurement error of these frequencies separately and E_{sim} is the measurement error for measurement for both pulsations simultaneously. All measurements are carried out at a mainstream velocity of $u_0=2\,\mathrm{m\,s^{-1}}$.

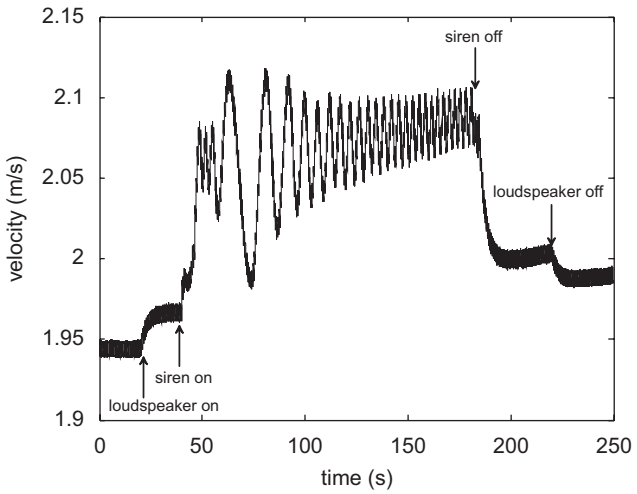

Fig. 8. Mainstream velocity of the flow measured with the turbine meter. After 20 seconds the loudspeaker is turned on at a frequency of 164 Hz, after another 20 seconds the siren is turned on at a frequency of about 164.2 Hz.

4.4. Measurements of velocity pulsation in the field

Determining the amplitude of the velocity pulsations using eight pressure transducers is not practical for industrial use of turbine flow meters. For this reason the options to measure the velocity amplitude by means of a hot wire or two pressure transducers embedded in the turbine meter has been investigated.

A hot wire determines the local velocity as well as velocity fluctuations, in the set-up where two hot wires are placed. Both hot wires are placed 1 cm upstream of the rotor and 1 cm from the pipe wall in the flow. One hot wire was placed in the wake of a vane of the flow straighteners and the other was placed in between two vanes (see Fig. 3). This was done to account for the effects of the complicated flow profile around the flow straightener. The mainstream velocity measured locally with the hot wires are higher than the mean velocity measured by the turbine meter. This is caused by hot wire measurements being local measurement, and as the

flow profile in the annulus is not uniform. The local flow velocity can be higher or lower than the mean velocity depending on the position of the hot wire. As expected the average velocity in the wake of the vane is lower than the velocity measured between the vanes of the flow straightener. The measured amplitude of the velocity pulsations for high velocities is within 10% of the amplitude of the velocity pulsations determined with the acoustical model, for low velocities, however, they are much less accurate. The velocity amplitude measured with the hot wire placed in the wake measures systematically a higher velocity amplitude than the other hot wire. This can probably be explained by the contribution of acoustically induced vortices shedding at the vane.

The velocity amplitude can also be calculated using the acoustical model described in Section 4.1 using just the two pressure transducers in the turbine meter. These calculations show that the velocity amplitude is predicted within 40%. This is not accurate enough for our tests, but can be used as an indication in practical situations.

5. Determination of the measurement error of the turbine meter

During a measurement the rotation speed of the rotor is recorded, without flow perturbations and with flow perturbations generated by the loudspeaker or the siren. The effect on the rotation speed, averaged over one revolution, is determined from a visual examination of the plots of the signals as shown in Fig. 9. In Fig. 9 the black oscillating line corresponds to the instantaneous reading of the flow meter. The smooth white line represents the measured velocity averaged over one rotation. The left figures show typical measurements for perturbations generated by the siren. The siren is turned on the first 30 s and then turned off. The right figures show typical results of measurements for the case in which perturbations are generated with the loudspeaker, starting with the speaker turned off, then turned on, subsequently turned off. Using a ruler deviations in the signal of 0.1% can be determined.

$$E_{\text{puls}} = \frac{\omega - \omega_0}{\omega_0}, \tag{23}$$

where ω is the angular velocity of the rotor while measuring pulsating flow and ω_0 is the angular velocity of the rotor for flow without pulsations. The variations of the pressure in the reservoir induces slow mass flow variations during a measurement (around 10^{-3} Hz). This is the main cause of inaccuracies in determining the measurement error of the flow meter.

The siren needs some time to reach a constant pulsation frequency, therefore these measurements are started with the siren already turned on. After the siren is turned off, this effect can also be seen. The slowing down of the siren causes the frequency to decay, possibly inducing pulsations that can momentarily cause a large oscillations in the measuring error during the transition. The influence of the pulsations is more accurately determined by using the loudspeaker. The loudspeaker is turned on and off during the measurement without complex transitional behaviour, making it easier to measure the effect of the pulsations. However, the loudspeaker could only be used at low flow velocities, up to $5\,\mathrm{m\,s^{-1}}$ in the main test pipe. Measurements carried out with the siren do match the corresponding measurements carried out with the loudspeaker.

6. Measurements

To investigate the effect of velocity pulsation on the flow measurements of the turbine meter, measurements were carried out at resonance frequencies of the set-up between 24 and 730 Hz and amplitudes of velocity pulsations ranging from small, $u_{\text{ac}}/u_0 \approx 0.01$, to very high amplitudes, $u_{\text{ac}}/u_0 \approx 2$. The turbine flow meter used in the set-up (Instromet type SM-RI-X G250) has a flow range from 20 to $400\,\mathrm{m^3\,h^{-1}}$ ($5.6\times 10^{-3}-0.11\,\mathrm{m^3\,s^{-1}}$), this corresponds to a velocity in the pipe of $u_0 = 0.7\,\mathrm{m\,s^{-1}}-13.3\,\mathrm{m\,s^{-1}}$. In our measurements velocities were varied from $u_0 = 0.5$ up to $15\,\mathrm{m\,s^{-1}}$. In Figs. 10 and 11 measurements are shown for a pulsation frequency of $f = 164$ Hz for different mainstream velocities. Both figures show exactly the same data set, however, in Fig. 10 the data are shown on a double logarithmic scale and in Fig. 11 the data are shown on a linear scale.

From these figures it is clear that for a large range of relative velocity amplitude extending over two decades and the range of main stream velocities, the measurements are still in fair agreement with the quasi-steady theory. We observe less than 40% deviation from the theory. By looking at the data, we can see that the deviation from the quasi-steady theory increases for decreasing main flow velocities. The effect of the Strouhal number and the Reynolds number will be discussed systematically in the next sections.

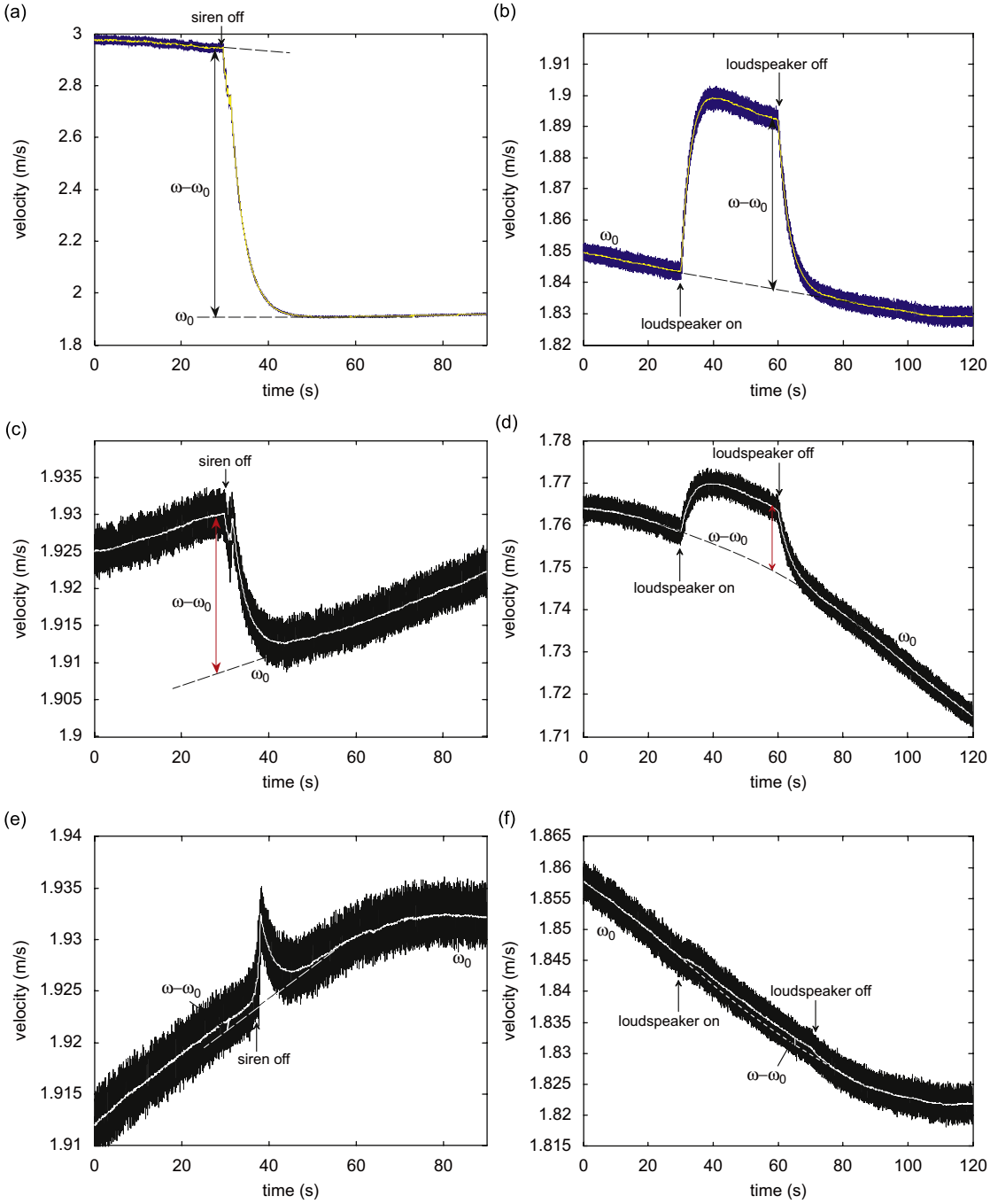

Fig. 9. The velocity measured with the turbine meter. The figures show some examples of different pulsation levels from extreme high (a,b) to low (e,f). Due to the long transient in the siren the influence of low pulsation levels cannot be detected (e) while they are still very clearly observable when the loudspeaker is used (f).

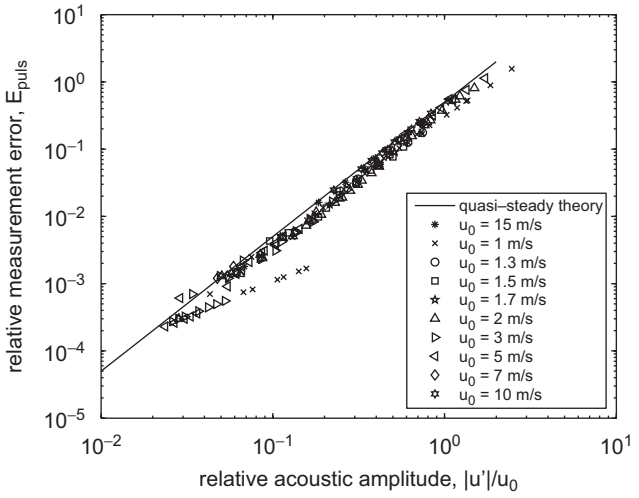

Fig. 10. The relative measurement error, E_{puls}, as a function of the relative amplitude of the pulsations, $|u'|/u_0$, for measurements at a frequency of 164 Hz. Plotted using double logarithmic scale.

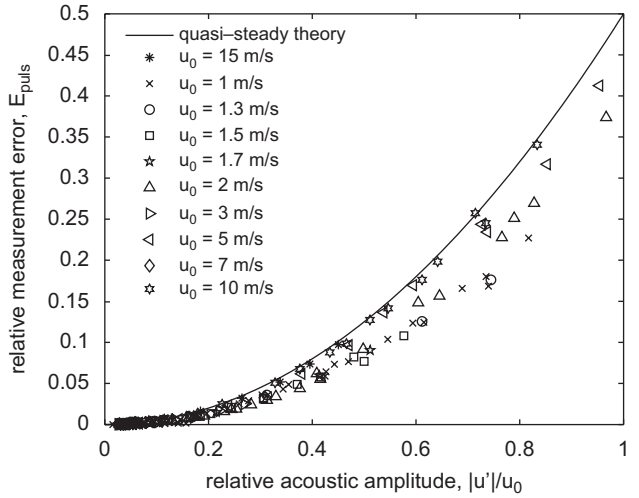

Fig. 11. The relative measurement error, E_{puls}, as a function of the relative amplitude of the pulsations, $|u'|/u_0$, for measurements at a frequency of 164 Hz.

6.1. Dependence on Strouhal number

In order to verify the range of validity of the quasi-steady theory, measurements have been carried out for a wide range of Strouhal numbers

$$Sr = \frac{fL_{\text{blade}}}{u_0}, \tag{24}$$

where $f = 1/T$ is the frequency of the pulsations, L_{blade} is the length of a rotor blade at the tip and u_0 is the main flow velocity at the position of the rotor. It is expected that for low Strouhal numbers the quasi-steady theory is valid. From Fig. 11, it is found that measurements for a given fixed frequency, f, and a fixed mainstream velocity, u_0, have a quadratic dependence on the relative velocity amplitude, u_{ac}/u_0. To investigate the dependence of the deviation in measured volume flow and actual flow E_{puls},

a quadratic function

$$E_{\text{puls}} = a\left(\frac{u_{\text{ac}}}{u_0}\right)^2, \tag{25}$$

was therefore fitted through the measured data at a given frequency, f, and flow velocity, u_0 using least-square fitting. The parameter a will be referred to as the "quadratic fit parameter". This parameter is $\frac{1}{2}$ for the quasi-steady theory. An example is shown in Fig. 12 for measurements at main stream velocity $u_0 = 1\,\text{m s}^{-1}$ and at frequency of pulsation $f = 164\,\text{Hz}$. We will consider only measurements with a relative amplitude $u_{\text{ac}}/u_0 < 1$ to obtain the quadratic dependence, because higher amplitudes no longer show the quadratic dependence. Measurements with relative amplitudes $u_{\text{ac}}/u_0 > 1$ are discussed separately.

In Fig. 13 the quadratic fit parameter, a, for the measurement at pulsation frequencies of 24, 69, 117 and 164 Hz and mainstream velocities from 1 to 15 m s^{-1} are plotted against Strouhal number. The error bar gives the 95% confidence level for the quadratic fit through the measured data. It is an indication for the quality of

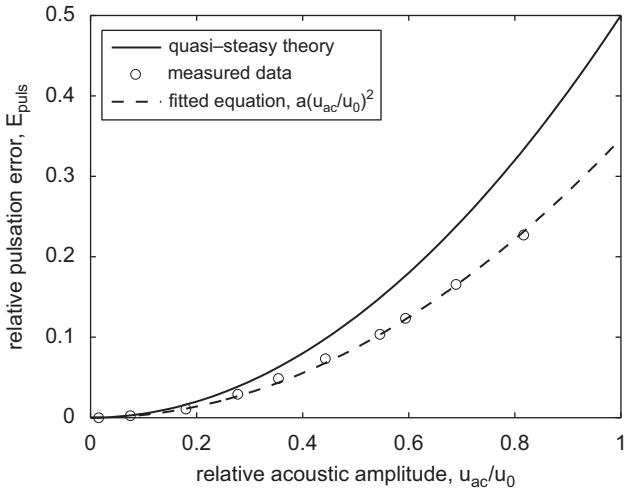

Fig. 12. A quadratic fit, $E_{\text{puls}} = a(u_{\text{ac}}/u_0)^2$ with $a = 0.35$ is shown for the measurement data at a mainstream velocity $u_0 = 1\,\text{m s}^{-1}$ and with pulsations of frequency $f = 164\,\text{Hz}$. Quasi-steady theory gives $a = 1/2$.

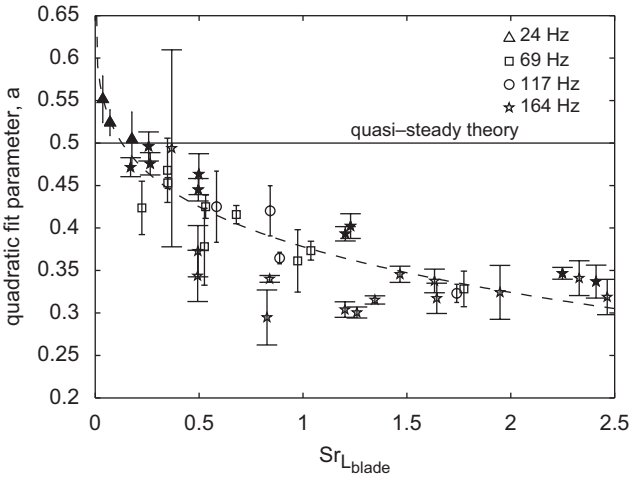

Fig. 13. The quadratic fit parameter a is plotted against Strouhal number for pulsation frequencies of 24, 69, 117 and 164 Hz and mainstream velocities from 1 to 15 m s^{-1}. The solid symbols represent the measurement using the siren, the open symbols the measurements using the loudspeaker.

the quadratic fit. The solid line in the figure shows the quadratic fit parameter, $a = 0.5$, for the quasi-steady theory, the dashed line is a function fitted through the data found from the present measurements. In Fig. 13 the data measured using the siren are solid symbols. The trends in the pulsation error measured with the siren and loudspeaker do not differ from each other. However around $Sr_{L_{\text{blade}}} = \text{O}(1)$, the siren data seems to have a slightly higher quadratic fit parameter than the loudspeaker data. An explanation for this could be that most of the measurements using the loudspeaker are for smaller relative amplitudes compared to the measurements using the siren. This indicates that at low amplitudes the pulsation error, E, is probably not exactly quadratically dependent on the velocity amplitude. The figure shows a clear Strouhal dependence, where the deviation from the actual flow decreases with increasing Strouhal number. However, the deviation from the actual volume flow stays within 40% of the quasi-steady theory for Strouhal number, $Sr_{L_{\text{blade}}}$, up to 2.5. Using regression, an equation is obtained to predict the dependence of $E_{\text{puls}} = a(u_{\text{ac}}/u_0)^2$ on the Strouhal number, $Sr_{L_{\text{blade}}}$:

$$a = -0.3672 Sr_{L_{\text{blade}}}^{\frac{1}{5}} + 0.7407 \quad \text{for } 0.05 \leqslant Sr_{L_{\text{blade}}} \leqslant 2.5. \tag{26}$$

This is a purely empirical relationship between the deviation and the Strouhal number, which cannot be explained theoretically. It is interesting to note that for $Sr_{L_{\text{blade}}} < 0.2$ we find $a > \frac{1}{2}$. We cannot explain this.

In Fig. 14 the data measured at the higher frequencies ($f = 360$ and 730 Hz) are shown separately, because they display different behaviour compared to the low-frequency data. The measurements at a pulsation frequency of 360 Hz all have a quadratic fit parameter, a, around 0.5. These measurements are closer to the deviation, E_{puls}, found by the quasi-steady theory than the equation found for the lower frequencies. The measurements at a pulsation frequency of 730 Hz show the same quadratic fit parameter for Strouhal numbers of around 6. However, at a Strouhal number of about 10 the data seems to support the empirical relation found using the lower pulsation frequencies. It is possible that these frequencies correspond to mechanical resonant frequencies of the turbine meter causing a different behaviour of the rotor.

Besides this, as explained in Section 4.3 for high frequencies small errors in the pressure can cause large errors in estimated acoustical velocity. This could explain some of the differences in Strouhal number dependence. Another possibility is that acoustical resonance hinder the measurements at these frequencies. When the length of the constriction caused by the core of the meter matches about half the wave length of the acoustical waves, there will be a resonance in this pipe segment. The length of this constriction is about 25 cm, i.e. this would give resonance frequencies of 680 Hz. For this resonance the rotor is close to a pressure

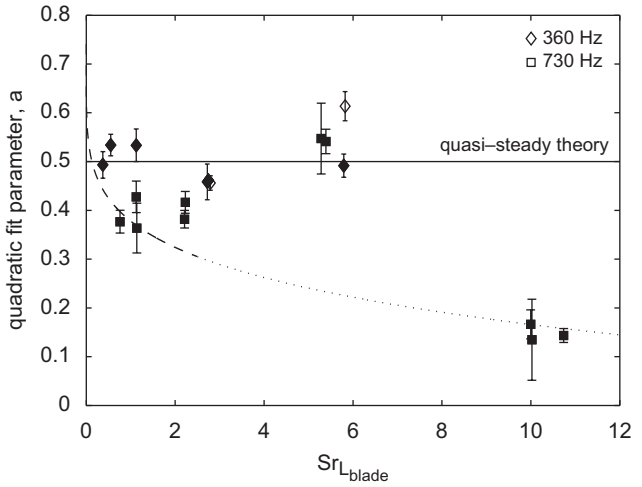

Fig. 14. The quadratic fit parameter a as a function of Strouhal number for pulsation frequencies of 360 and 730 Hz. The '◇' show the data of measurements at pulsation frequencies of 360 Hz, the '□' show the data of measurements at pulsation frequencies of 730 Hz. The solid symbols represent the measurements using the siren, the open symbols the measurements using the loudspeaker.

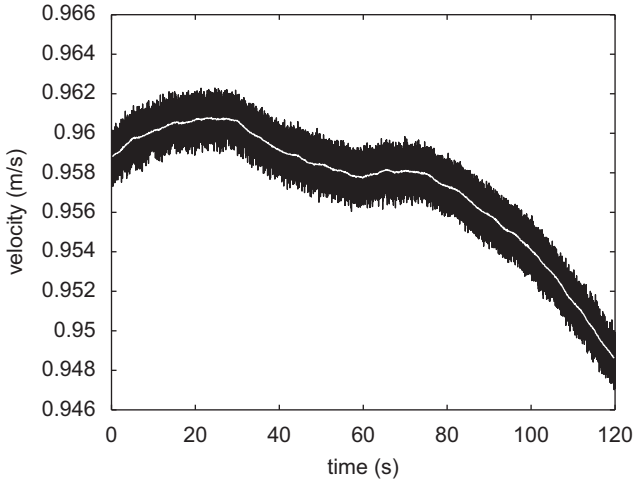

Fig. 15. Some measurements at low velocities and high frequency show a negative measurement error. The loudspeaker is turned on after 30 s inducing pulsations of 730 Hz, after another 30 s the loudspeaker is turned off.

antinode which corresponds to conditions in which the acoustical velocity at the turbine is difficult to determine.

To exclude the possibility that the hollow space inside the flow straightener could act as a Helmholtz resonator, this area was filled with foam. This did not change the observed response of the flow meter to pulsations.

Care was taken to prevent these problems occurring at high frequencies by excluding measurements for which the rotor was close to a pressure antinode.[1] To be able to draw more conclusions for the deviation, E_{puls}, at Strouhal numbers greater than 2.5, additional measurements are necessary.

At high frequencies, 367 and 730 Hz, other strange phenomena can be found; at low pulsation levels, $|u'|/u_0 \leqslant 0.1$. A negative measurement error can be observed for low velocities, up to $2\,\text{m}\,\text{s}^{-1}$ (see Fig. 15, in this plot the velocity of the flow measured by the turbine meter is given, the smooth white line represents the velocity averaged over one revolution of the turbine meter). These errors do not always reproduce. We suspect here a combination of mechanical vibration and friction. During our tests dust particles were present in the flow and this affected the friction in the rotor. However, tests after cleaning the rotor indicated that this had only a minor effect on most of our data. No significant effect is found for $u_0 > 2\,\text{m}\,\text{s}^{-1}$.

6.2. Dependence on Reynolds number

To investigate if there is also a dependence of the deviation, E_{puls}, on the Reynolds number, $Re_{L_{\text{blade}}}$, the residual of the Strouhal number dependence predicted by the empirical relation (Eq. (26)) and the quadratic fit parameter found for the measurements are plotted as a function of Reynolds number, $Re_{L_{\text{blade}}}$, for pulsation frequencies of 24, 69, 117 and 164 Hz (see Fig. 16).

Fig. 16 shows no significant correlation, between the Reynolds number and the difference between the measurements and the empirical relation for the Strouhal number dependence. We conclude that there is no significant dependence of the Reynolds number, $Re_{L_{\text{blade}}}$, on the deviation, E_{puls}.

6.3. High relative acoustic amplitudes

Several measurements were carried out at relative pulsation amplitudes larger than unity; $u_{\text{ac}}/u_0 > 1$. Such high pulsation levels are not likely to occur in practice. However, to investigate the range of the applicability of

[1]Note that all measurements between 360 and 730 Hz have been rejected because of a very large scatter in the quadratic fit coefficient a, which was related to difficulties in the measurement of the acoustical velocity.

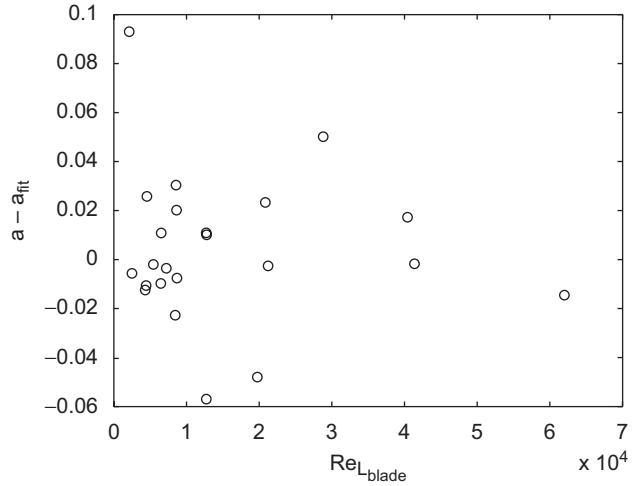

Fig. 16. The difference between the quadratic fit parameter found for the measured data, a and the quadratic fit parameter found by the empirical relation in Section 6.1, a_{fit}, is plotted as a function of Reynolds number for pulsation frequencies of 24, 69, 117 and 164 Hz.

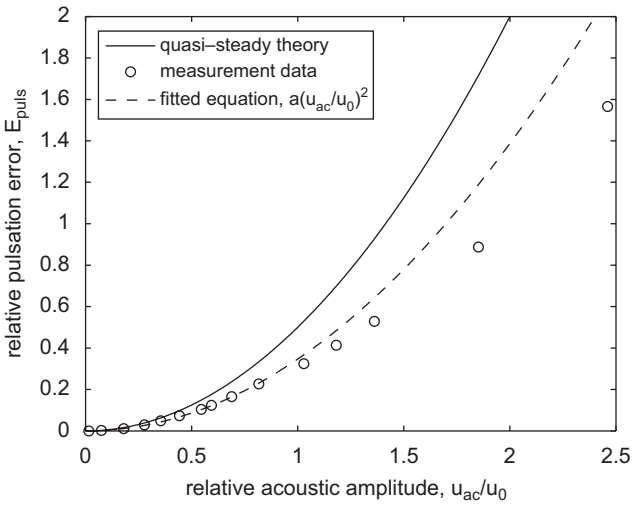

Fig. 17. The deviation, E_{puls} as a function of the relative acoustic amplitude, u_{ac}/u_0. A quadratic fit, $E_{\text{puls}} = a(u_{\text{ac}}/u_0)^2$ derived for $u_{\text{ac}}/u_0 < 1$ (with $a = 0.35$) is shown for the measurement data at a mainstream velocity $u_0 = 1\,\text{m}\,\text{s}^{-1}$ and with pulsations of frequency $f = 164\,\text{Hz}$.

the quasi-steady theory, it is interesting to look at these results. At these high amplitudes the deviation, E_{puls}, can no longer be described by the quadratic dependence found for lower amplitudes. In general the measured deviation, E_{puls}, is smaller less than the deviation found by extrapolation of the quadratic dependence found for $u_{\text{ac}}/u_0 < 1$. The difference with this quadratic dependence is still small for relative acoustic amplitudes $u_{\text{ac}}/u_0 \approx 1$ and increases for increasing amplitude. Typical measurement data are shown in Fig. 17. At pulsation levels $u_{\text{ac}}/u_0 < 1$, the quasi-steady theory overestimates the effect of pulsations by about a factor 1.4. At pulsation levels $u_{\text{ac}}/u_0 \backsimeq 2.5$ the effect of pulsations is overestimated by a factor 2. At such high amplitudes, flow reversal will certainly occur.

6.4. *Influence of the shape of the rotor blades*

The influence of the shape of the blade was investigated by replacing the standard rotor with rotor with a different blade shape. The original rotor has blades with a rounded upstream leading edge and a chamfered

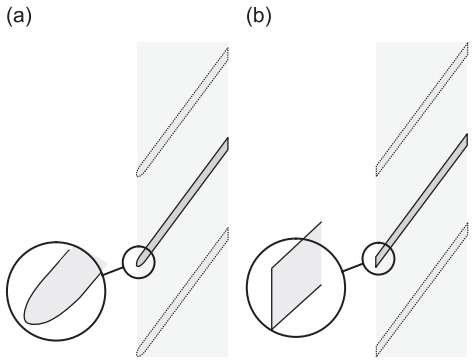

Fig. 18. A schematic drawing of the rotor (a) with rounded leading edges and (b) with a chamfered leading edges used in the measurements.

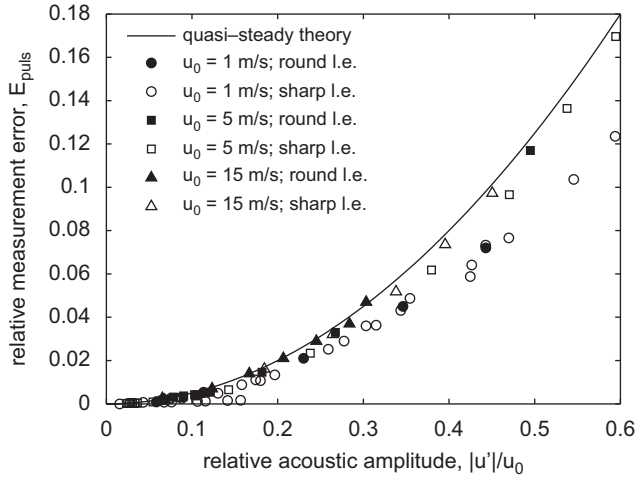

Fig. 19. The relative measurement error, E_{puls}, is plotted against the relative pulsation amplitude, $|u'|/u_0$, for measurements with the 'new' rotor with chamfered-leading-edge blades and the standard rotor with rounded-leading-edge blades. The data are for measurements at a pulsation frequency of 164 Hz and mainstream velocities, $u_0 = 1$, 5 and 15 m s^{-1}.

trailing edge. This rotor was replaced by a rotor with chamfered leading edges similar to the trailing edges (Fig. 18). We refer to this 'new' rotor as the symmetric rotor.

To determine the behaviour of the rotor with chamfered leading edges in pulsating flow some of the measurements carried out with the standard rotor are repeated using the new rotor. Fig. 19 shows the results of the measurements carried out at a pulsation frequency of 164 Hz and mainstream velocities of $u_0 = 1$, 5 and 15 m s^{-1}, compared to the measurement data obtained for the standard rotor. In Fig. 19 the solid symbols are the data measured with the rotor with chamfered-leading-edge blades. Within the accuracy of the measurement no difference was found. To verify this further a quadratic fit as explained in Section 6.1 was made and this parameter was plotted against Strouhal number, $Sr_{L_{blade}}$ for low frequencies ($f = 24$, 69, 117 and 164 Hz) (Fig. 20). Again, we see that within the accuracy level of the measurements there is no difference between the deviation of the volume flow measurement for the rotor with blades with rounded leading edges and the rotor with blades with chamfered leading edges.

7. Conclusions

The effect of the pulsating flow on a turbine flow meter has been investigated experimentally and results have been compared to the results of a simplified quasi-steady model. A set-up was built making it is possible

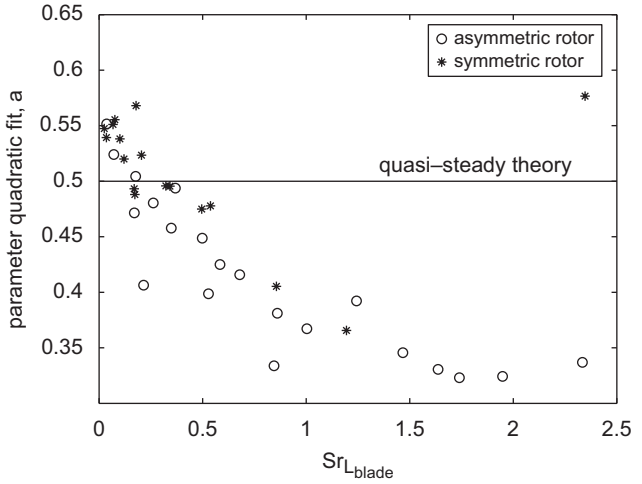

Fig. 20. The quadratic fit parameter a is plotted against Strouhal number for pulsation frequencies of 24, 69, 117 and 164 Hz and mainstream velocities from 1 to 15 m s^{-1}. The 'o' represents the measured data of the standard rotor with blades with rounded leading edges and '$*$' represents the data measured with the 'new' rotor with blades with chamfered leading edges. Again, no difference can be found within measurement accuracies for the two rotors.

to induce pulsations with a frequency from 24 to 730 Hz, relative acoustic velocity amplitudes, u_{ac}/u_0, from 2×10^{-2} up to 2 and volume flows ranging from the minimum to the maximum flow specified by the manufacturer, i.e. from 20 to 400 m^3 h^{-1}. Multi-microphone measurements have been used to determine the amplitude of the velocity pulsation at the rotor. The error caused by the pulsations is obtained from the comparison of the rotation speed of the rotor in presence of pulsations with the one in the case where there are no pulsations. The measurements show that the simplified quasi-steady theory gives a fair approximation of the error caused by the pulsations. The measurements agree with the theory within 40% for nearly all measurements, even for measurements at high relative acoustical amplitudes. Even when flow reversal occurs $u_{ac}/u_0 \backsimeq 2.5$ the quasi-steady theory still provides a rough estimate of the error. We found that the error caused by pulsations is dependent on Strouhal number. For $Sr_{L_{blade}} < 2.5$ an empirical relation was found for the dependence of the error on the Strouhal number. Intuitively one expects that the influence of pulsations should decrease with increasing pulsation Strouhal number. This corresponds to our observations. As yet no physical explanation is found for this specific dependence. For $Sr_{L_{blade}} > 2.5$ the behaviour of the rotor is still unclear, caused by the difficulties in measuring at higher pulsations frequencies. We still observe a significant pulsation error up to $Sr_{L_{blade}} = 10$ at which we intuitively would expect that such effect would average out. The measurement error caused by the pulsations is not significantly dependent on the Reynolds number. The shape of the upstream edge of the rotor blades does not influence the Strouhal number dependence of the systematic error induced by the pulsations. The theory predicts very well the effect of simultaneous acoustical perturbations with different frequencies.

This study stresses the importance of determining the acoustical velocity at the rotor for a correction of measurement errors due to pulsations. Measurements with local velocity probes such as hot wires are difficult to use because they do not distinguish between local vortical perturbations and global acoustical waves. Acoustical waves can be detected by means of microphones mounted flush in the wall. This would however involve multiple microphones at a certain position to allow the detection of the plane waves by cross-correlation method analogous to microphone array techniques.

Acknowledgements

This research was financially supported by the technology foundation STW (grant ESF.5645).

References

[1] K. Atkinson, A software tool to calculate the over-registration error of a turbine meter in pulsating flow, *Flow Measurement and Instrumentation* 3 (3) (1992) 167–172.
[2] R. Cheesewright, K. Atkinson, C. Clark, G. ter Horst, R. Mottram, J. Viljeer, Field tests of correction procedures for turbine flowmeters in pulsatile flows, *Flow Measurement and Instrumentation* 7 (1996) 7–17.
[3] H. Dijstelbergen, Dynamic response of turbine flowmeters, *Instrument Review* 13 (1966) 214–245.
[4] B. Lee, R. Cheesewright, C. Clark, The dynamic response of turbine flowmeters in liquid flows, *Flow Measurement and Instrumentation* 15 (2004) 239–248.
[5] W. Jungowski, M. Weiss, Effects of flow pulsation on a single-rotor turbine meter, *Journal of Fluids Engineering* 118 (1996) 198–201.
[6] R.J. McKee, Pulsation effects on single- and two-rotor turbine meters, *Flow Measurement and Instrumentation* 3 (1992) 151–166.
[7] F. Weinig, Theory of two-dimensional flow through cascades, in: W. Hawthorne (Ed.), *Aerodynamics of Turbines and Compressors Vol. X of High Speed Aerodynamics and Jet Propulsion*, Princeton University Press, 1964, pp. 13–82.
[8] R. Cheesewright, D. Edwards, C. Clark, Measurements with a turbine flow meter in the presence of large, non-sinusoidal pulsations, *Proceedings of Fourth International Symposium on Fluid Control, Fluid Measurement and Visualization*, Toulouse, 1994.
[9] M. Peters, Aeroacoustic Sources in Internal Flows, PhD Thesis. Technische Universiteit Eindhoven, 1993.
[10] G. Kirchhoff, Uber den einfluss der wärmtelettung in einem gase auf die schallbewegung, *Annalen der Physik and Chemie* 73 (1868) 383–406.
[11] H. Tijdeman, On the propagation of sound in cylindrical tubes, *Journal of Sound and Vibration* 39 (1975) 1–33.
[12] A.D. Pierce, *Acoustics, an Introduction to its Physical Principles and Applications*, McGraw-Hill, New York, 1989.
[13] M. Peters, A. Hirschberg, A. Reijnen, A. Wijnands, Damping and reflection coefficient measurements for an open pipe at low Mach and low Helmoltz numbers, *Journal of Fluid Mechanics* 256 (36) (1993) 499–534.
[14] D. Ronneberger, C. Ahrens, Wall shear stress caused by small amplitude perturbations of turbulent boundary-layer flow: an experimental investigation, *Journal of Fluid Mechanics* 3 (83) (1977) 433–464.
[15] S. Allam, M. Åbom, Investigation of damping and radiation using full plane wave decomposition in ducts, *Journal of Sound and Vibration* 292 (2006) 519–534.
[16] G Hofmans, Vortex Sounds in Confined Flows, PhD Thesis. Technische Universiteit Eindhoven, 1998.